Environmental Science & Technology

pubs.acs.org/est

Article

Unravelling Coupled Hydrological and Geochemical Controls on Long-Term Nitrogen Enrichment in a Large River Basin

Ying Liang, Rui Ma,* Henning Prommer, Qing-Long Fu, Xue Jiang, Yiqun Gan, and Yanxin Wang

Cite This: https://doi.org/10.1021/acs.est.4c05015

Read Online

ACCESS | Metrics & More | Article Recommendations | Supporting Information

ABSTRACT: Many groundwater and surface water bodies around the world show a puzzling and often steady increase in nitrogen (N) concentrations, despite a significant decline of agricultural N inputs. This study uses a combination of long-term hydrogeochemical and hydraulic monitoring, molecular characterization of dissolved organic matter (DOM), column experiment, and reactive transport modeling to unravel the processes controlling N-reactive transport and mass budgets under the impacts of dynamic hydrologic conditions at a field site in the central Yangtze River Basin. Our analysis shows that the desorption of ammonium (NH_4^+) from sediments via cation exchange reactions dominates N mobilization and aqueous N concentrations, while the mineralization of organic N compounds plays only a minor role. The reactive transport modeling results illustrate the important role of cation exchange reactions that are induced by temporary NH_4^+ input and cation concentration changes under the impact of both seasonal and long-term hydrologic variations. Historically, cation exchangers have acted as efficient storage devices and mitigated the impacts of high levels of NH_4^+ input. The NH_4^+ residing on cation exchanger sites later acts as a long-term N source to waters with the delayed desorption of sediment-bound NH_4^+ induced by the change of hydrologic conditions. Our results highlight the complex linkages between highly variable hydrologic conditions and NH_4^+ partitioning in near-surface, river-derived sediments.

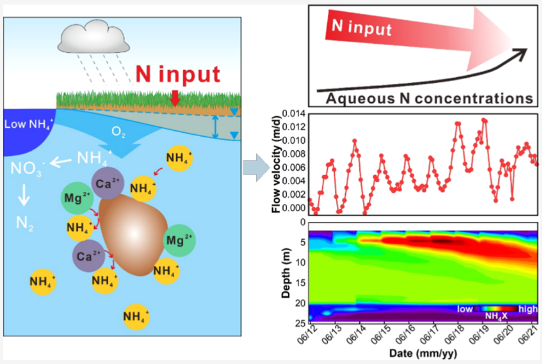

KEYWORDS: *nitrogen cycling, groundwater surface water interaction, reactive transport, cation exchange*

INTRODUCTION

Excessive nitrogen (N) in groundwater is a prevalent problem worldwide due to the adverse effects on water quality and aquatic ecosystem health.[1−5] It is particularly severe in aquifers beneath agricultural areas, where nitrate (NO_3^-) is often the main groundwater contaminant.[2,3,6−12] Elevated ammonium (NH_4^+) concentrations generally persist in reducing environments, while oxidation to NO_3^- through nitrification occurs where O_2 becomes available.[5,6,13−15] In many instances, NH_4^+ containing groundwater discharge has shown to serve as a substantial N source for surface water bodies, where it induces eutrophication.[6,16−18]

Increasing N concentrations in groundwaters and surface waters have been reported for various settings, despite declining N inputs. It was thereby ascribed to the transient storage of N in sediments.[2,3,10,19] Often, N-containing organic compounds were considered as the predominant form of N stored in the sediments of aquatic systems such as wetlands, estuaries, and river deltas.[3,11,20] Correspondingly, it has been hypothesized that NH_4^+ is primarily released to groundwater in response to the decomposition and release of sediment organic N.[1,3,4,10,11] Meanwhile, there is growing evidence that sediment-bound NH_4^+ could play a considerable role and that sorption/desorption of NH_4^+ via cation exchange reactions could significantly influence groundwater NH_4^+ concentrations.[16,21,22] Fine-grained riparian sediments potentially serve as an important temporary storage pool for NH_4^+.[7,14,17,23−27] This has, for instance, been observed in sediments from the Red River Delta plain and the Pearl River Delta, where deeper sediments have been shown to contain up to hundreds of mg of NH_4 per kg.[1,28] Furthermore, some studies have also found that exchangeable NH_4^+ (the sediment-bound NH_4^+ that can be extracted with KCl solution at room temperature) is particularly enriched in near-surface sediments, where its content has shown to be 1 order of magnitude higher than that of porewater NH_4^+ concentration.[7,22,29] However, the role and relevance of NH_4^+ sorption and desorption on N cycling are still not more broadly recognized and possibly severely underestimated in many, if not most, previous field studies.

Received: May 22, 2024
Revised: October 21, 2024
Accepted: October 21, 2024

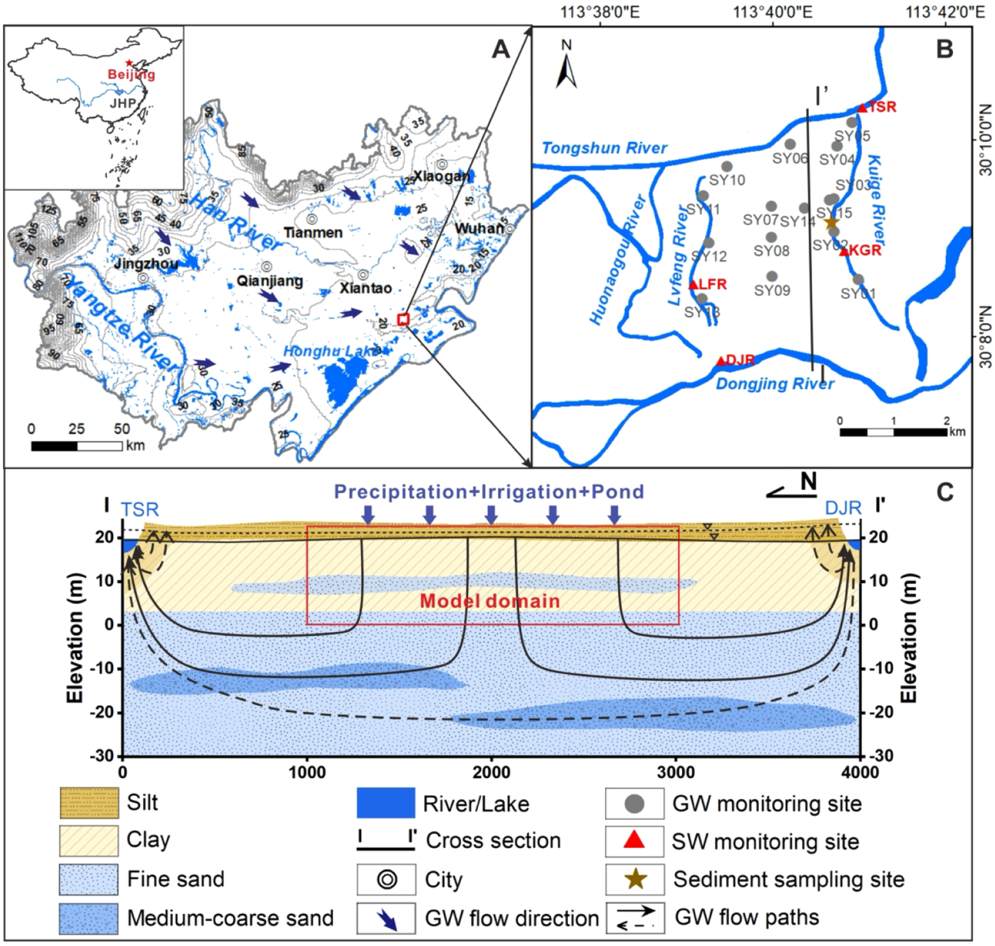

Figure 1. (A) Location of JHP and regional groundwater flow, (B) the Shahu monitoring site, and (C) hydrogeological cross section in which groundwater flow paths are indicated as dotted lines for wet season conditions and as solid lines for conditions during the dry season. TSR and DJR refer to the Tongshun River and the Dongjing River, respectively.

In riparian zones and other systems, where seasonal groundwater and surface water interactions occur, highly dynamic exchange fluxes can trigger complex hydrogeochemical interactions[30−33] and subsequently alter N-associated biological processes.[15,34−37] A similarly complicating factor might be the occurrence of temporary upward fluxes in arid climates, where evapotranspiration exceeds rainfall, which can strongly impact the migration rate of contaminants, including NO_3^-, in the vadose zone and in shallow aquifers.[38,39] Significant repartitioning of NH_4^+ between sediment and aqueous phases might occur in response to changes of water chemistries induced by groundwater and surface water interactions.[16,23,26] Several recent studies have demonstrated that recharge with oxygenated surface waters may enhance NH_4^+ attenuation by promoting nitrification.[13,14,40] Furthermore, sorption of NH_4^+ onto aquifer sediments is likely promoted during discharge of NH_4^+-bearing groundwater,[23] and the long-term accumulation of NH_4^+ is commonly observed in aquifer systems experiencing intensive groundwater−surface water interactions.[6,13,14,16]

Here, we investigate the hypothesis that storage and release of N in sediments via cation exchange may be the key process responsible for the persistence of a high N concentration in surface and groundwater bodies, long after excessive agricultural N inputs have ceased. This hypothesis is derived from long-term hydrogeochemical monitoring, observed sediment-bound (sorbed) N, and laboratory-scale column experiments with molecular characterization of DOM. Constrained by the field observations, we use reactive transport modeling to analyze and reveal the mechanisms controlling transient N storage and its release in aquifers under variable hydrologic conditions in a large river basin. Our results demonstrate that dynamic hydrologic conditions enhance enrichment of NH_4^+ in sediments and its later release is promoted by shifting water chemistries, which in turn affects N-cycle processes and long-term water quality.

■ MATERIALS AND METHODS

Study Site. The Shahu site is located in the southeast of the Jianghan Plain (JHP), encompassing an area of approximately 10 km^2. Within the study area, monitoring wells were installed at 13 locations; at each location, 3 nested monitoring wells were screened at depths of 10, 25, and 50 m, respectively. The 10 m wells were screened in the upper aquitard, which is characterized by a relatively low permeability with a hydraulic conductivity of ∼10^{-8} m/s, whereas the 25 and 50 m wells were screened in the underlying sandy and considerably more permeable confined aquifer with hydraulic conductivity between ∼10^{-6} m/s and ∼10^{-4} m/s.[13,41−43]

The seasonal groundwater level fluctuations at the Shahu site are mainly induced by variations in precipitation rates, irrigation patterns, and pond infiltration as well as river−

https://doi.org/10.1021/acs.est.4c05015
Environ. Sci. Technol. XXXX, XXX, XXX−XXX

groundwater interaction. The Tongshun River (TSR), Dongjing River (DJR), Lvfeng River (LFR), and Kuige River (KGR) are embedded within the low-permeability upper aquitard and, thus, only affect groundwater levels locally, i.e., within several tens of meters away from these rivers.[41,44]

Over several decades, the Shahu site has been subject to intensive agricultural activity, and consequently, high levels of groundwater NH_4^+ have been observed.[4,13,27] Due to shifts in agricultural practices, fertilizer use has significantly declined since 2012. However, both NH_4^+ and NO_3^- concentrations have remained high and have indeed even increased in surface and groundwaters (Figure S1). A detailed description of the study site can be found in Text S1.

Data Collection. At the Shahu site, the measurements of piezometric heads and river stages as well as sampling of groundwater and surface water were conducted approximately monthly from June 2012 to September 2014[13] and from June 2018 to July 2019 (Figure 1). The sediment core was collected in March 2021 at the Eastern JHP from a newly drilled bore from a depth of ∼28 m below the land surface (BLS). Full details on water level monitoring and sample collection are provided in Text S1.

Water Analysis. In situ analyses of physicochemical parameters, including water temperature, pH, electrical conductivity (EC), oxidation−reduction potential (ORP), dissolved oxygen (DO), and alkalinity, as well as concentrations of redox constituents, including total Fe, Fe^{2+}, sulfide (S^{2-}), NH_4^+, and NO_2^- were conducted. Concentrations of major cations, anions, and dissolved organic carbon (DOC) in the water samples were determined by standard methods. All details of the applied sample preservation and analytical techniques are described in Text S1.

Sediment Characterization. All sediment samples were oven-dried to measure the bulk density, moisture content, specific surface area (SSA), cation exchange capacity (CEC),[45] and bulk mineral and elemental compositions. Additionally, the extraction of sediment-bound NH_4^+ was conducted by field-moist sediments. Water-soluble sediment-bound organic matter (WSOM) was extracted from dried sediments to analyze DOC concentration and molecular characterization. Details of the extraction techniques for sediment-bound NH_4^+ and WSOM can be found in Text S2.

FT-ICR MS Analysis and Data Processing. The molecular characterization of DOM was determined by a 7.0-T Fourier transform ion cyclotron resonance mass spectrometer (FT-ICR MS) with the range of m/z set at 100−1000 for all WSOM samples. The DOM molecular composition for each sample was interpreted by the FTMSDeu Code. The full data processing details are provided by Zhou et al.[46] Content of DON in each sediment sample was subsequently calculated by multiplying the N/C ratio by DOC concentration. Details on the FT-ICR MS analysis and data processing can be found in Text S3.

Column Experiment. Dried sediment samples were packed into three identical columns (10 cm in length and 2.6 cm in diameter). After presaturated with deionized water, all columns were flushed with 5 pore volumes (PVs) of artificial irrigation water (AIW), containing 5.5 mM NH_4^+, 1 mM Br^-, and DO in equilibrium with the atmosphere, to mimic a high NH_4^+ input period. Varying influent compositions were applied to simulate differing scenarios of groundwater−surface water interactions: (i) column A: surface water infiltration simulated by the injection of artificial surface water (ASW), (ii) column B: groundwater discharge simulated by the injection of artificial groundwater (AGW), and (iii) column C: alternating injection of ASW and AGW after every 2 PVs to simulate the frequent exchange between surface water and groundwater. The ASW contained 0.05 mM NH_4^+ and 0.15 mM NO_3^- in equilibrium with the atmosphere, corresponding to the average measured surface water composition (Figure S2). While the AGW contained 0.5 mM NH_4^+ and DO-free on the basis of typical shallow groundwater composition.[13] Detailed experiment procedures and hydrochemical compositions are provided in Text S4 and Table S1, respectively. In total, 45 PVs of feed solutions were passed through each of the experimental columns to investigate the long-term behavior of the N-reactive transport.

Conceptual Hydrogeological Model. At the Shahu site, in the shallow aquifer sections, particularly the upper aquitard, groundwater flow, and groundwater flow paths are controlled by local-scale groundwater−surface water interactions (Figure 1B,C). The model domain defined for our reactive transport simulations represents the local-scale processes in the saturated groundwater zone away from the rivers (i.e., TSR, DJR, LVR, and KGR, see Figure 1B). There, groundwater flow predominantly occurs in the vertical direction. It was therefore idealized as a column in which transient flow and, accordingly, reactive transport occur at variable rates. The shallow groundwater zone is generally recharged by a combination of rainfall and infiltration of surface waters, the latter including ponds and irrigation water. Measured groundwater levels show that upward hydraulic gradients from the confined aquifer into the overlying low-permeability zones occurred only sparsely during seasonal fluctuations of groundwater levels and at a much smaller magnitude compared to the predominating downward hydraulic gradient.[47] From 2017 onward, a continued decline in groundwater levels in the confined aquifer induced an increased downward vertical hydraulic gradient in the shallow aquifer zone, therefore enhancing surface water infiltration.

Numerical Modeling Tools and Approaches. A multicomponent reactive transport model was set up for a comprehensive analysis of the geochemical response to the hydrological interactions between surface water and groundwater from June 2012 to September 2021. MODFLOW[48] and PHT3D[49] were used for simulating coupled flow, transport, and geochemical processes under the dynamic hydraulic conditions and the associated intensive exchange of surface water and groundwater. Since vertical flow is the key hydrological driver of the reactive transport processes at the Shahu site, a one-dimensional (1D) model was developed to represent the vertical groundwater flow and reactive transport processes. The model domain extends over 25 m and is discretized into 22 layers (the top layer is 4 m thick, while the layers below have a uniform thickness of 1 m), thereby covering the aquitard and connecting to the uppermost part of the confined aquifer (Figure 1).

Groundwater Flow. Initial estimates of hydrogeologic properties and hydraulic parameters were adopted from previous studies[41,42] and subsequently adjusted within plausible ranges during calibration against our field observations. All employed physical parameters of the groundwater flow model are listed in Table S2.

The hydraulic conductivity and the recharge rate were calibrated according to the observed groundwater level data. Detailed monthly recharge rates are listed in Figure S3. A drain

https://doi.org/10.1021/acs.est.4c05015
Environ. Sci. Technol. XXXX, XXX, XXX−XXX

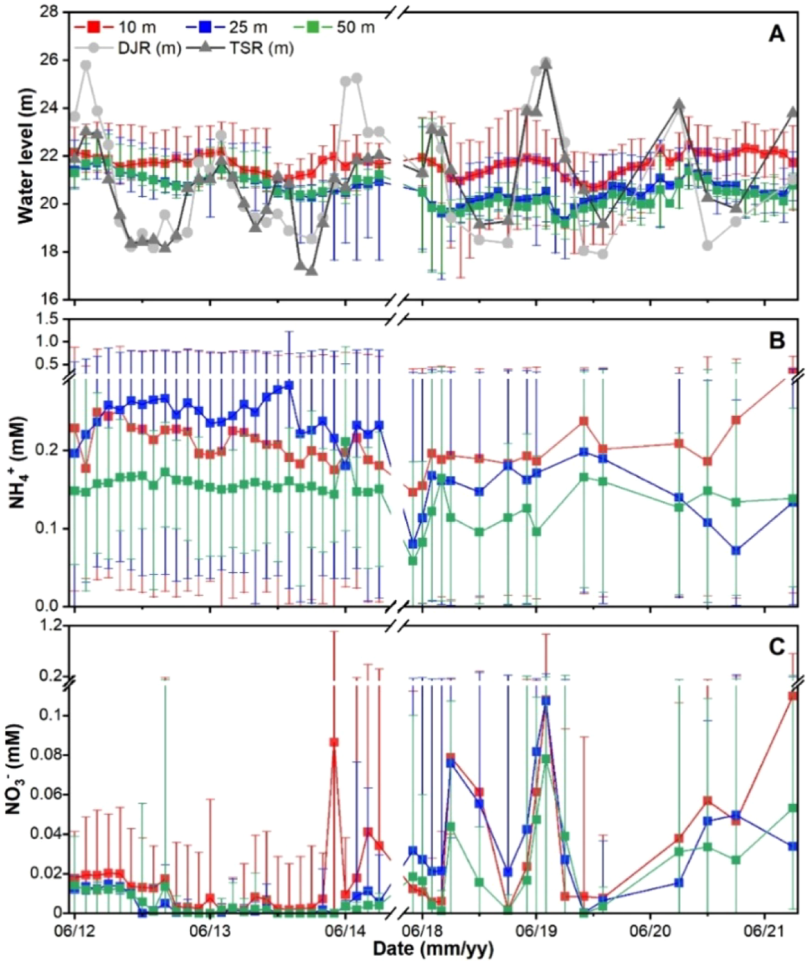

Figure 2. (A) Groundwater levels and river stages, (B) NH_4^+ concentration, and (C) NO_3^- concentrations change along with time at the Shahu site in the discharge area of JHP. Two whisker ends represent minimum and maximum, and solid squares show the mean values.

with an elevation of 20.1 m allows groundwater to discharge. The bottom boundary of the model domain was defined by the time-varying Constant-Head (CHD) Package, based on the averaged monthly groundwater levels observed at the 25 m wells (Figure S3).

Geochemical Reaction Network. The standard PHREEQC database[49−51] was used as a starting point for assembling a problem-specific reaction network of equilibrium and kinetically controlled reactions that potentially affect the mobilization and attenuation of various N species. Additional reactions were formulated to consider the kinetically controlled biodegradation of organic matter by multiple electron acceptors, including O_2, NO_3^-, SO_4^{2-}, and ferrihydrite(s). On the other hand, all-included cation exchange reactions (i.e., $Ca^{2+} + 2X^- \leftrightarrow CaX_2$, $Mg^{2+} + 2X^- \leftrightarrow MgX_2$, $Na^+ + X^- \leftrightarrow NaX$, $K^+ + X^- \leftrightarrow KX$, and $NH_4^+ + X^- \leftrightarrow NH_4X$) were directly adopted from the PHREEQC standard database. The thermodynamic constants are listed in Table S3.

In the following, we largely focus on the description and discussion of the newly appended reactions. Both nitrification and denitrification were considered to play critical roles in N cycling, based on previous evidence for these reactions to occur in the study area.[6,13]

Similar to previous modeling studies in related hydrochemical systems,[52] biodegradation of organic matter was modeled by employing a partial equilibrium approach (PEA), in which it is assumed that organic matter oxidation is the rate-limiting step, and the consumption of electron acceptors can therefore be quantified as equilibrium reaction.[40,50,53−55] The electron acceptors are automatically consumed according to their thermodynamic favorability. This implies that denitrification[34,37,40,55]

$$4NO_3^- + 5CH_2O + 4H^+ \rightarrow 2N_2 + 7H_2O + 5CO_2$$

is inhibited as long as aerobic respiration

$$CH_2O + O_2 \rightarrow H_2O + CO_2$$

still proceeds.

$$NH_4^+ + 2O_2 \rightarrow NO_3^- + H_2O + 2H^+$$

Nitrification was also assumed to be kinetically controlled and to proceed in the presence of DO. The full list of rate expressions and parameters that were incorporated into the reaction database to quantify the kinetically controlled oxidation of organic matter and nitrification is provided in Text S5 and Table S4. Finally, the mineralization of N-containing DOM was not included because of the negligible concentrations that were detected in both surface water and groundwater samples.[13]

Reactive Transport Model. Field-observed water compositions were used to define four discrete zones (0−4 m, 4−7m, 7−20 m, and 20−25 m depth, respectively) of initial water

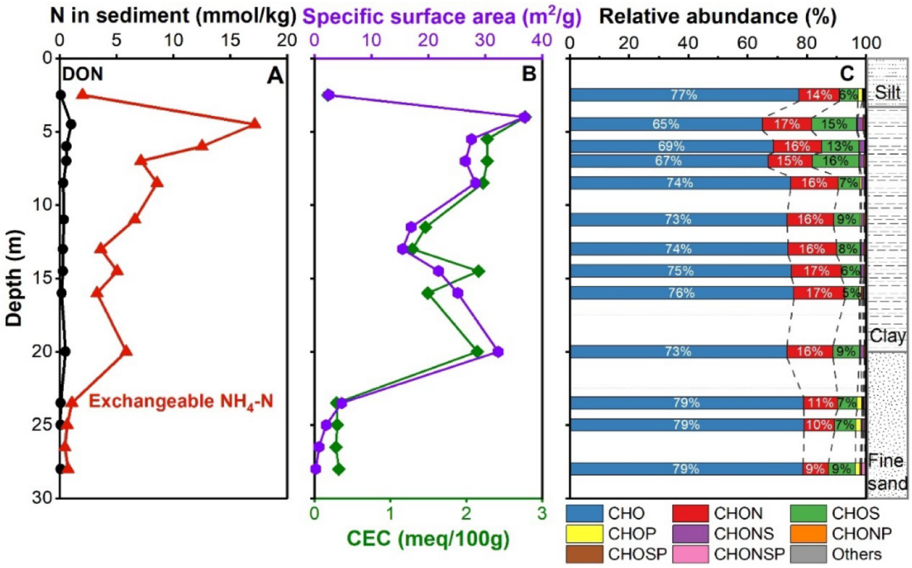

Figure 3. Vertical distribution of (A) DON and exchangeable NH_4^+ concentrations, (B) measured cation exchange capacity (CEC) and specific surface area (SSA), and (C) relative abundance of DOM formulas extracted from sediment collected from the Shahu site located in the JHP discharge area. Clay-rich sediments at depth from 4.5 to 20 m showed 1 order of magnitude higher CEC and SSA values than the silty and sandy sediments.

compositions at the start of the simulations. The initial concentrations of the considered N species, major ions, and DOC were assigned according to measured concentrations (Table S5). Two minerals were included in the reaction network, calcite, and ferrihydrite, both as equilibrium phase minerals that were assumed to be present at the start of the simulations. The initial concentration contents of calcite and ferrihydrite were estimated from X-ray diffraction (XRD) and X-ray fluorescence (XRF) results (Figure S4 and S5) as well as reported data in existing studies.[56,57] Furthermore, the CECs applied in the model were adopted from measured, site-specific values. Subsequently, the initial exchanger occupancy was determined through equilibration with the initial water compositions and thus varied from zone to zone.

Fertilizer applications associated with irrigation and subsequent infiltration of irrigated water are the primary pathway for N entering the aquifer underlying the agricultural area. Our previous investigations indicate that fertilizer-derived N prevailing in irrigation recharge water generally occurs as NH_4^+ in the JHP.[6,13] Thus, NH_4^+ was assumed to be the main form of N loading to the groundwater system. In the model, time-varying hydrochemical compositions were defined as model boundary conditions, thereby reflecting both seasonal changes and long-term input trends. The application of fertilizers was normally performed in May of each year; thus, the recharge water compositions for this period were correspondingly characterized by high concentrations of NH_4^+. In other months, NH_4^+ was absent from groundwater recharge. The time-varying recharge water compositions assigned at the top boundary corresponded to the observed surface water composition, thus reflecting the distinct differences between dry and wet seasons, respectively. The detailed seasonal cycle of recharge water compositions is illustrated in Figure S6. To capture the long-term trend of decreasing anthropogenic NH_4^+ input caused by changing agricultural practices at the JHP, a gradual change in NH_4^+ concentration from 4 mM in 2011 to 1 mM in 2020 was applied to the recharge water compositions representing irrigation seasons (Figure S6). The groundwater chemistry at the model bottom boundary was adopted from the measured groundwater composition at the 25 m wells.

To unravel and illustrate the importance of various key reactions and hydrologic conditions on N-reactive transport, a range of conceptual model variants were considered:

Case 1: Considering all the above reactions under field-observed hydrologic conditions (base case),

Case 2: Nonreactive transport of solutes (no geochemical reactions) under field-observed hydrologic conditions,

Case 3: As case 1, except for the exclusion of cation exchange reactions,

Case 4: Reactions as in case 1, but assuming a constant hydraulic gradient over the entire simulation period, excluding seasonal hydrological dynamics,

Case 5: Reactions as in case 1, but assuming a self-repeating seasonally varying flow (with a constant average hydraulic gradient), and

Case 6: Reactions as in case 1, but assuming a successively changing hydraulic gradient without the occurrence of seasonal changes.

RESULTS

Temporal Variations of Hydrologic Condition and Water Chemistry in Different Seasons. The Shahu site is characterized by seasonal fluctuations of river stages that can reach 8 m. Groundwater level variations, particularly at 10 m depth, closely coincide with the river stage fluctuations but were attenuated to 1−2 m (Figure 2A). Furthermore, groundwater levels show a decreasing trend from 2012 to 2014 to 2018−2020, especially at 25 and 50 m depths, before increasing again in 2020−2021 (Figure 2A). The vertical hydraulic gradients generally increased in 2018−2021 compared to those in 2012−2014.[13]

In response to the hydrological processes and their variations, both transport- and reaction-induced hydrochemical changes occurred over the monitoring period. NO_3^- concentrations at all depths (10, 25, and 50 m wells) increased

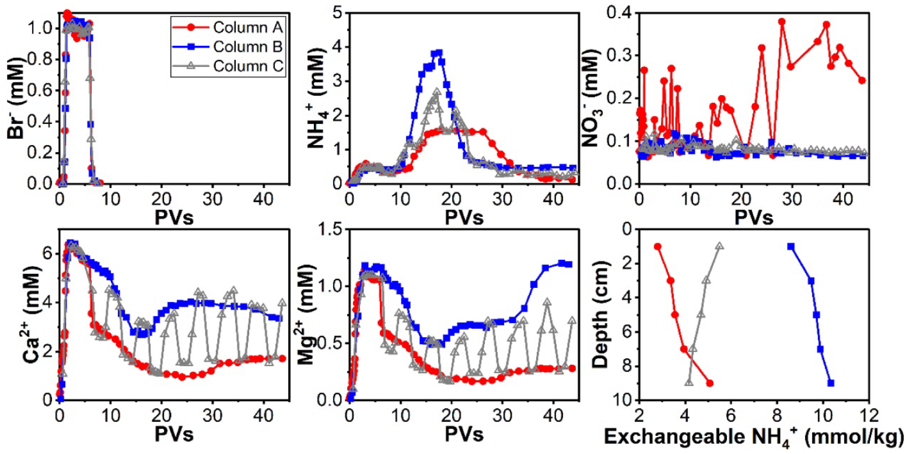

Figure 4. Breakthrough curves of Br, NH_4^+, NO_3^-, Ca, and Mg in columns A, B, and C, as well as exchangeable NH_4^+ concentrations in the sediments at the end of the experiments.

over time, even though the fertilizer-associated N input was significantly reduced over this period (Figure 2C). NH_4^+ concentrations at 10 m depth remained initially constant from 2012 to 2014 but then showed an increase in the 2018−2021 data, while at 25 and 50 m depth, the concentrations showed a decrease in the 2018−2021 period. Surface waters, such as river water, pond, and irrigation waters within the Shahu site, show similar, but seasonally varying, major ion compositions (Figure S2). Higher concentrations of Ca^{2+} and Mg^{2+} usually occurred during the wet seasons (between April and July), while the NO_3^- concentrations and pH values were higher during the dry seasons (between December and March). Compared to the groundwater hydrochemical compositions, surface waters were generally characterized by lower NH_4^+, Ca^{2+}, and Mg^{2+} concentrations and higher NO_3^- and Cl^- concentrations and pH values (Figure S2). NO_3^- concentrations in surface waters were 1 order of magnitude higher than those in groundwaters, especially during the period of 2018−2021. The concentrations of Ca^{2+}, Mg^{2+}, and HCO_3^- decreased and K^+ and Cl^- concentrations and pH significantly increased in groundwaters in the 2018−2021 period compared to the 2012−2014 period.

Storage of N in Sediments. Sediment samples collected from the Shahu site showed relatively high exchangeable NH_4^+ concentrations, varying between 0.46 and 17.14 mmol/kg (Figure 3A). Notably, higher concentrations of exchangeable NH_4^+ usually occurred in clay-rich sediments, with an average content of 7.75 mmol/kg. Vertically, near-surface sediment generally had higher concentrations of exchangeable NH_4^+, peaking at a depth of ∼5 m.

Vertically, CEC and SSA of sediment samples at the Shahu site showed a very similar depth profile. Low CEC and SSA values were found at depth <4 m, similar to depth >20 m, where sandy sediments prevail. Sediment samples collected at a depth of 4.5 m showed the highest values for CEC (2.78 mequiv/100g) and SSA (36.9 m^2/g) (Figure 3B).

Generally, N-containing DOM molecules showed a relative abundance below 10%. The relative abundance of CHON formulas ranged from 9% to 17%, therefore comparatively lower than CHO formulas (Figure 3C). Calculated DON contents ranged between 0.10 and 1.12 mmol/kg, peaking at a depth of ∼5 m, similar to the depth of the peak exchangeable NH_4^+ concentration occurred. Importantly, the maximum exchangeable NH_4^+ concentration is more than 16 times higher than that of DON (Figure 3A). Thus, exchangeable NH_4^+ clearly dominates the sediment N pool rather than DON. As shown in Figure S7, most of the CHON molecules of high relative abundance were determined to be lignin, and therefore of limited bioavailability, since their H/C ratio is <1.5.[58]

Solute Transport Behavior Observed in Column Experiments. Conservative solute transport, as indicated by Br, exhibited identical behavior in all three columns. Br^- was detected at ∼1 PV and approached injected concentration after ∼1.4 PVs (Figure 4). In comparison, NH_4^+ reached peak concentrations much slower than that of Br^-. Effluent NH_4^+ concentration remained low for more than 8 PVs, before starting to increase. After breakthrough (∼10 PVs), effluent NH_4^+ concentrations remained much lower than the injected concentrations, particularly in column A, where ASW was injected, and concentrations peaked at ∼1.6 mM. However, NO_3^- concentrations in the effluent were higher than the injected concentrations. Column B, in which AGW was injected, exhibited a higher NH_4^+ peak concentration of ∼3.8 mM.

The observed breakthrough behavior of NH_4^+ shows to be linked with the changes in Ca^{2+} and Mg^{2+} concentrations. NH_4^+ concentration increased in concert with decreasing Ca^{2+} and Mg^{2+} concentrations, while conversely, there was a notable decrease in NH_4^+ concentrations with increasing Ca^{2+} and Mg^{2+} concentrations. Sediments sampled from column B displayed the highest exchangeable NH_4^+ concentrations after the end of the experiment. Accumulation of exchangeable NH_4^+ was also observed in the sediments of column C, which was exposed to the alternating injection, particularly in the top of the column. On the other hand, in column C, exchangeable NH_4^+ concentrations in the sediments were even below the initial concentration at depths between 0 and 6 cm.

Reactive Transport Modeling. Recharge to the deeper groundwater zones mainly occurs during wet seasons (Figure S3A). The resulting observed water level dynamics were captured well by the simulated groundwater levels at both 10 and 25 m depths (Figure S3B). Accordingly, the simulated flow velocities at 10 m depth fluctuate seasonally. In addition, the simulations also capture the increased downward flows induced by increasing head gradients (case 1 in Figure S3C).

The reactive transport model simulations that considered the full set of biogeochemical reactions (case 1) reproduce the

https://doi.org/10.1021/acs.est.4c05015
Environ. Sci. Technol. XXXX, XXX, XXX−XXX

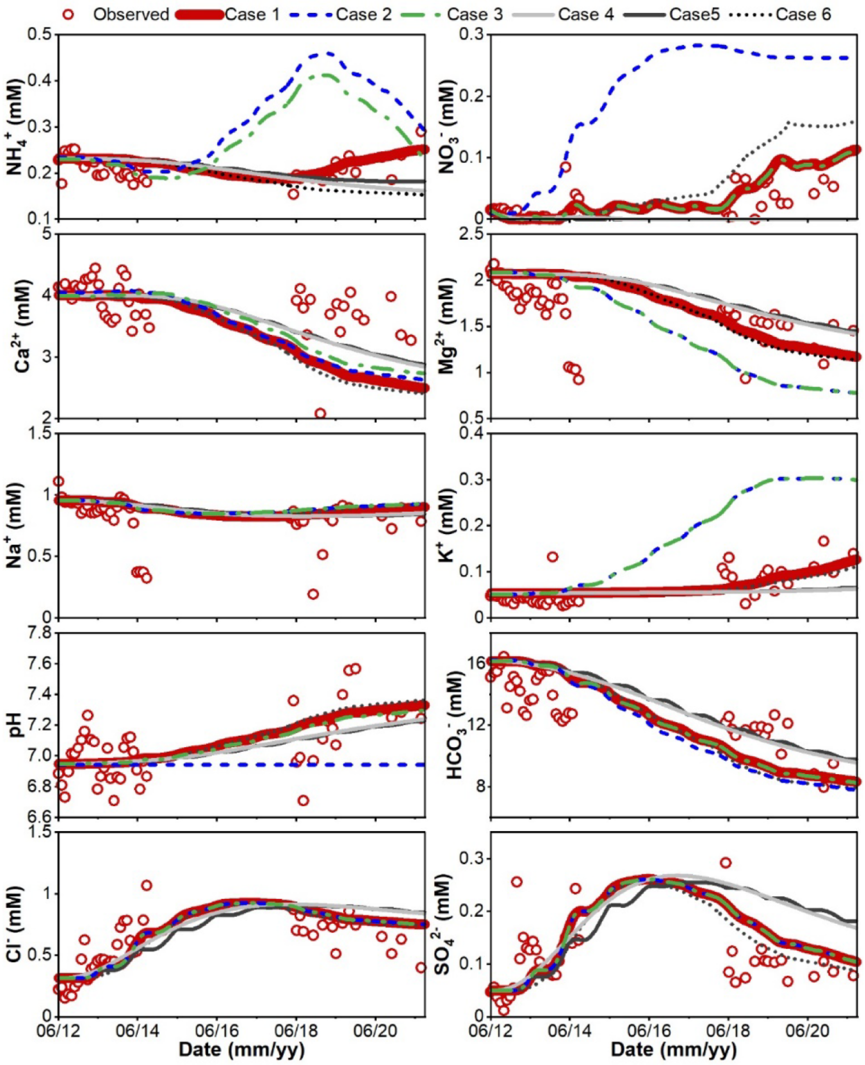

Figure 5. Comparison of results from different reactive/nonreactive model variants with observation data for major ions, N species (NH_4^+ and NO_3^-), and pH at 10 m depth. The observed data shown represent the averaged values from 13 monitoring wells.

field-observed concentration trends for most major ions (Ca^{2+}, Mg^{2+}, Na^+, K^+, NH_4^+, SO_4^{2-}, Cl^-, HCO_3^-, and NO_3^-) and pH reasonably well (Figure 5), therefore suggesting that the hypothesized conceptual hydrogeological and hydrogeochemical model is highly plausible. In contrast, the corresponding nonreactive transport simulations (case 2), where all geochemical processes were switched off, and also the reactive transport model variant (Case 3) that solely excluded cation exchange reactions from the full reaction network employed in Case 1, failed to match field observations.

Similarly, the model variants that either assumed (i) a constant hydraulic gradient (case 4), (ii) constant averaged yearly hydraulic gradients with seasonal dynamic (case 5), or (iii) observed yearly hydraulic gradients without seasonal dynamic (case 6) could neither capture the NH_4^+ and NO_3^- transport behavior or observe the major ion concentrations, such as Ca^{2+}, Mg^{2+}, HCO_3^-, and SO_4^{2-}, and pH, especially in the later part of the simulation period.

The accumulation of NH_4^+ on exchanger sites, particularly in clay-rich sediments, is indicated in Figure 6. While the simulated NH_4X concentrations were relatively low (~0.3 mM) in the earlier part of the simulation period, they increased after June 2014, eventually reaching up to 0.6 mM. The NH_4X concentration at a depth of ~5 m was almost doubled during the simulation period, before a slight decline occurred after 2021 in the near-surface clay-rich sediments.

The decrease of MgX_2 occurs during the increase of NH_4X that is accumulating during the intrusion of NH_4^+ with the infiltrating surface water, which was enhanced, while vertical hydraulic gradients increased after 2014 (Figure 6 and S7). Note that NaX and KX concentrations were approximately 1 order of magnitude lower than those of CaX_2 and MgX_2 (Figure S8).

DISCUSSION

Prominent Role of Cation Exchange on Controlling Ammonium Storage and Release in JHP. Our sediment analysis shows that exchangeable NH_4^+ concentrations are relatively high and approximately 1 order of magnitude higher than DON-hosted N concentrations (Figure 4A). Importantly, this contrasts with many previous studies suggesting that DOM is the predominant form of N storage and accordingly for long-term N release from sediments.[1,4,11] Characterization of near-surface clay-rich sediments collected in this area show their large CECs and SSAs, which promotes NH_4^+ sorption.[20,42] The elevated CEC values and the high exchangeable NH_4^+

https://doi.org/10.1021/acs.est.4c05015
Environ. Sci. Technol. XXXX, XXX, XXX−XXX

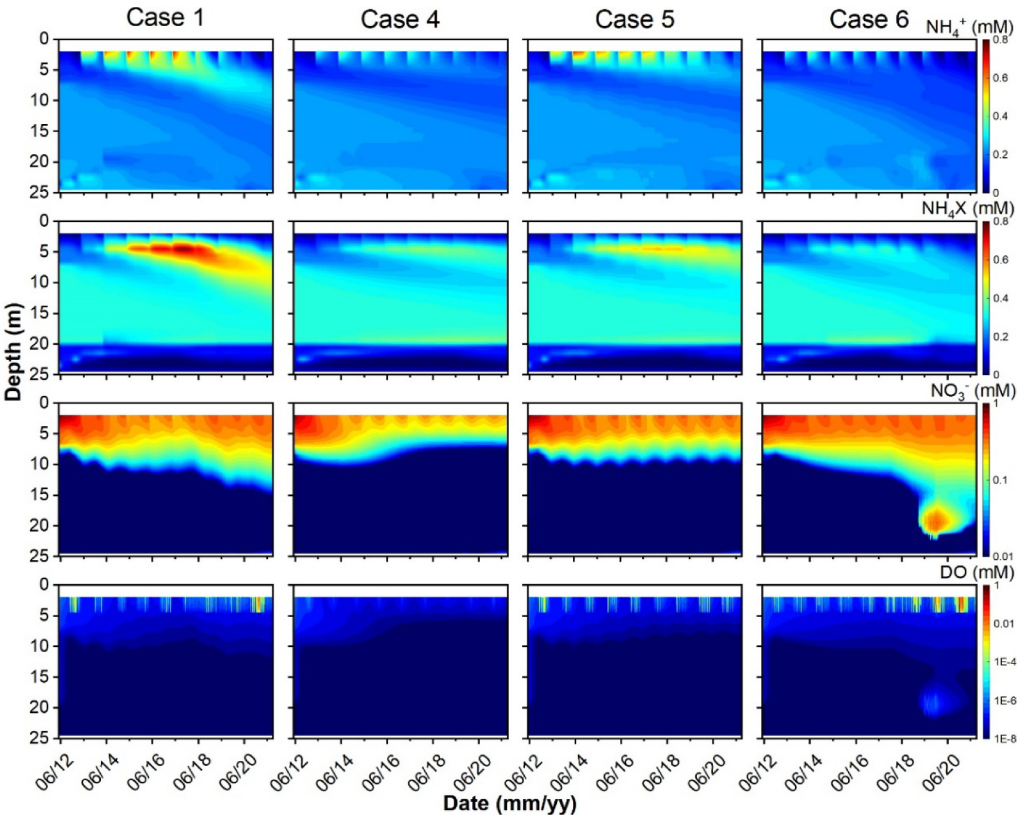

Figure 6. Comparison of the concentrations of groundwater NH_4^+, NO_3^-, and DO, as well as sediment-bound NH_4^+ (NH_4X) between models with different hydrologic conditions.

concentrations strongly suggest that cation exchange plays a dominant role in the transient storage of N in sediments and as a regulator for aqueous N concentrations. This finding complements the results of previous studies that noted the absence of significant organic N concentrations,[13] therefore attributing a minor role of DON decomposition in controlling aqueous N concentrations.

The important role of cation exchange for NH_4^+ storage and release is further underpinned by the results of both the reactive transport simulations and column experiments. With respect to the former, key evidence is provided by the comparison of the reactive transport simulation results (case 1) with those from the corresponding conservative model (case 2), and the case where only cation exchange reactions were excluded (case 3). Only the full reactive transport model was able to match the majority of the observed hydrochemical patterns, while the other model variants failed to match particularly the observed cation concentrations. The retarded breakthrough of NH_4^+ in the complementary column experiments, in concert with declining Ca^{2+} and Mg^{2+} concentrations, provides further supporting evidence for the role of cation exchange in N storage.

The observed increase of aqueous NO_3^- concentrations at all monitoring wells, which coincides with the observed decrease of groundwater NH_4^+, particularly at the monitoring wells screened in the confined aquifer (Figure 3), suggests that nitrification is another important reaction affecting N-cycling. It is promoted under the more oxidized conditions created by infiltrating surface water.[7,13,15] Observed effluent NO_3^- concentrations that were higher than the influent concentration in the column experiments, particularly in the column with aerobic ASW influent composition, also confirm the occurrence of nitrification (Figure 3). Subsequently, most of the NO_3^- produced was removed via denitrification in the anoxic zone, causing an obvious N mass loss during the experiments. The main reactive transport model variant in which nitrification-denitrification was considered (case 1) captures the observed NO_3^- variations and, therefore, supports the hypothesis that nitrification-denitrification controls groundwater NO_3^- concentrations.

Seasonal Hydrological Dynamics Control N Enrichment in Shallow Groundwater. As the rates at which recharge to the shallow aquifer occurred followed a seasonal pattern, this also implied seasonally varying downward hydraulic gradients and magnitudes of flow velocities (Figures 2 and S3). The alternating chemical compositions of the surface waters cause the periodic change in groundwater chemistry at shallow depth (<10 m) (Figure S9). The distinct NH_4^+ adsorption/desorption behavior that is induced at the Shahu site and its link with the alternating compositions of the recharged water are mimicked by the corresponding column experiments, i.e., under controlled conditions (column C in Figure 3). The comparison of modeling results obtained for case 1, which considers the seasonal flow dynamics, and case 6, which assumes an equivalent but steady recharge rate, illustrates the importance of the seasonal dynamics on the N-reactive transport behavior. In the former case, inflow of aerobic surface water (DO $\geq$ 0.4 mM) during the dry season while downward flow rates are slow constrains the extent of the oxic zone, where nitrification can occur, to shallow groundwater depths <4 m (Figure 6). In comparison, the much higher downward flow velocities during the wet season, i.e., while

https://doi.org/10.1021/acs.est.4c05015
Environ. Sci. Technol. XXXX, XXX, XXX−XXX

fertilizers are utilized, leads to an enhanced N mass loading and downward transport of NH_4^+ (Figure S10) without the opportunity for nitrification to occur due to absence of oxygen (DO < 0.01 mM). Thus, the seasonal hydrological dynamics largely suppressed the nitrification of NH_4^+ to NO_3^- and facilitated NH_4^+ preservation at depths between 4 and 10 m, where groundwater remains anoxic during the dry and wet seasons (Figure S10). This finding contrasts previous studies, which suggested that slowly moving NH_4^+ could be largely consumed by nitrification during groundwater residence.[16] The relevance of the seasonal dynamics is illustrated by the modeling results for case 6, which did not consider the dynamics and as a consequence underestimated NH_4^+ concentrations and overestimated NO_3^- concentrations in the shallow groundwater zone.

Overall, there is combined evidence from field observations, column experiments, and reactive transport modeling (case 1) that the seasonal alteration of the recharge water composition in combination with the variations in flow velocities initially enhances the storage of NH_4^+ in the near-surface clay-rich sediments at the depth around 5 m (Figures 3 and 6). In more recent years, however, the release of adsorbed NH_4^+ from clay-rich sediments via cation exchange sustained elevated groundwater NH_4^+ concentrations at the shallow depth (<10 m), even though N inputs from fertilizer applications decreased or ceased during this period (Figure S1).

Impact of Long-Term Increased Downward Hydraulic Gradient on Ammonium Desorption and Aqueous N Concentrations. Enhanced surface water infiltration induced by a long-term decline in groundwater levels, attributed to human activities such as groundwater pumping, has been observed at the Shahu site (Figure S3)[47] and also reported for other regions.[59−61] There, the enhanced recharge of surface waters in the period between 2018 and 2020 caused a shift to more oxidized conditions at shallow depth <4 m, compared to the earlier monitoring period (Figure 6), leading to more NO_3^- produced via nitrification. Due to the increased downward hydraulic gradients, transport of NO_3^- to deeper groundwater was enhanced (Figure 6). This explains the observed increase of NO_3^- concentrations at 10 m depth and further below. In comparison, the downward movement of near-surface produced NH_4^+ was retarded by cation exchange, whereby the long-term trend of decreased Ca^{2+} and Mg^{2+} concentrations promoted NH_4^+ sorption and its enrichment in sediment at depths of around 10 m (Figures 5 and 6). Thus, the downward movement of NH_4^+ was further prohibited, leading to the dilution of aqueous NH_4^+ at greater depth. This resulted in the decrease of NH_4^+ concentrations in groundwater zones at the >10 m depths (Figures 4 and 6). The changes of groundwater NH_4^+ and NO_3^- concentrations along the profile are more complex than those reported in previous studies, which suggested that surface water infiltration would efficiently lower groundwater NH_4^+ concentrations by dilution and promotion of nitrification reaction.[7,17,40]

The role of the long-term increased downward hydraulic gradient in controlling N concentrations is illustrated by comparing model results for case 1 with those for cases 4 and 5. The model variants, which did not consider the enhanced vertical hydraulic gradients (cases 4 and 5) and their induced change in geochemical conditions (i.e., concentrations of O_2 and major ions), were unable to capture the trend of increasing NH_4^+ concentrations at 10 m depth, neither with nor without considering seasonal hydrological dynamics, and underestimating both aqueous NH_4^+ and NO_3^- concentrations (Figure 5).

IMPLICATIONS

Despite changes in agricultural practices, N remains one of the most concerning diffuse groundwater contaminants, and understanding the physical and hydrogeochemical processes that control its transit time in large catchments is key for developing and adapting water management practices. Our study highlights the importance of exchangeable NH_4^+ as the most important N pool for groundwaters in an intensely studied large river basin, the JHP, therefore contrasting many studies that attributed N-related water quality deterioration to sediment-hosted DON. Through multiple lines of evidence, combining field, lab, and modeling studies, we illustrate the importance of N release from sediment-bound exchangeable NH_4^+ on groundwater quality under the impact of dynamic hydrologic conditions.

Fertilizer applications for agricultural activities are common in many large river basins around the world, which often exhibit seasonal or other hydrological dynamics induced by groundwater and surface water interaction.[5,13,14,54] For the past decades, the intervention actions that have been taken to reduce riverine nutrient loading in large river basins such as the Mississippi, Susquehanna and Songhuajiang River Basins, failed in many cases to achieve the expected water quality improvements, similar to what occurred at the JHP study site.[2,3,9,10] Previous studies attributed the time lag between reduced N inputs and delayed water quality improvement to legacy N accumulated in soils and groundwater.[3,11,62] However, it remained unclear under what conditions the sorption/desorption of NH_4^+ is promoted and how it affects long-term water quality. Our simulating results now demonstrate that seasonal hydrological dynamics, coupled with geochemical processes, can enhance N enrichment in shallow subsurface sediments and sustain high levels of N release into groundwaters at later times. Large river basins that have a similar fertilizer application history to the JHP are likely to store large masses of N in groundwater zones, as NH_4^+, and experience a delayed release of N to water bodies, especially where hydrologic conditions change, for example, through (over)extraction of groundwater and/or climate change impacts. Thus, water resource management must consider the transient storage and release of N and its long-term effect, and long-term continuous hydrological and chemical monitoring networks are required for better predicting water quality change in large river basins. This study deepens our broader understanding of long-term water quality changes in large river basins and the necessary steps for a better water quality management.

ASSOCIATED CONTENT

Supporting Information

The Supporting Information is available free of charge at https://pubs.acs.org/doi/10.1021/acs.est.4c05015.

Texts describing study site, water level monitoring, water and sediment sampling, sample analysis, column experiments, and reactive transport modeling (Texts S1−S5); tables summarizing the hydrochemical compositions of artificial influent water applied in column experiments and the parameters and initial conditions of the reactive transport model (Tables S1−S5); the trends of N

https://doi.org/10.1021/acs.est.4c05015
Environ. Sci. Technol. XXXX, XXX, XXX−XXX

concentrations in waters and fertilizer use over the past decades (Figure S1); groundwater and surface water chemistry variation over time (Figure S2); flow model setup and simulation results (Figure S3); XRD and XRF results (Figures S4–S5); recharge concentration of model variants (Figure S6); Van Krevelen diagrams of DOM molecules extracted from sediments (Figure S7); simulating results for sediment-bound cations, aqueous cations, and NH_4^+ and NO_3^- concentrations (Figures S8–S10) (PDF)

AUTHOR INFORMATION

Corresponding Author

Rui Ma – *Hubei Key Laboratory of Yangtze River Basin Environmental Aquatic Science, School of Environmental Studies, China University of Geosciences, Wuhan 430074, China; State Key Laboratory of Biogeology and Environmental Geology, China University of Geosciences, Wuhan 430074, China*; Email: rma@cug.edu.cn

Authors

Ying Liang – *Hubei Key Laboratory of Yangtze River Basin Environmental Aquatic Science, School of Environmental Studies, China University of Geosciences, Wuhan 430074, China; State Key Laboratory of Biogeology and Environmental Geology, China University of Geosciences, Wuhan 430074, China;* orcid.org/0009-0006-2153-4599

Henning Prommer – *School of Earth Sciences, University of Western Australia, Crawley, Western Australia 6009, Australia*

Qing-Long Fu – *Hubei Key Laboratory of Yangtze River Basin Environmental Aquatic Science, School of Environmental Studies, China University of Geosciences, Wuhan 430074, China;* orcid.org/0000-0002-7125-6877

Xue Jiang – *Hubei Key Laboratory of Yangtze River Basin Environmental Aquatic Science, School of Environmental Studies, China University of Geosciences, Wuhan 430074, China*

Yiqun Gan – *Hubei Key Laboratory of Yangtze River Basin Environmental Aquatic Science, School of Environmental Studies, China University of Geosciences, Wuhan 430074, China*

Yanxin Wang – *Hubei Key Laboratory of Yangtze River Basin Environmental Aquatic Science, School of Environmental Studies, China University of Geosciences, Wuhan 430074, China*

Complete contact information is available at: https://pubs.acs.org/10.1021/acs.est.4c05015

Notes

The authors declare no competing financial interest.

ACKNOWLEDGMENTS

This study was financially supported by the National Natural Science Foundation of China (Grant no. 42425207 and 42407102) and the Ministry of Education of China (Grant no. B18049).

REFERENCES

(1) Jiao, J. J.; Wang, Y.; Cherry, J. A.; Wang, X.; Zhi, B.; Du, H.; Wen, D. Abnormally High Ammonium of Natural Origin in a Coastal Aquifer-Aquitard System in the Pearl River Delta, China. *Environ. Sci. Technol.* **2010**, *44* (19), 7470–7475.

(2) Van Meter, K. J.; Van Cappellen, P.; Basu, N. B. Legacy Nitrogen May Prevent Achievement of Water Quality Goals in the Gulf of Mexico. *Science* **2018**, *360* (6387), 427–430.

(3) Chen, D.; Hu, M.; Dahlgren, R. A. A Dynamic Watershed Model for Determining the Effects of Transient Storage on Nitrogen Export to Rivers. *Water Resour. Res.* **2014**, *50* (10), 7714–7730.

(4) Du, Y.; Deng, Y.; Ma, T.; Xu, Y.; Tao, Y.; Huang, Y.; Liu, R.; Wang, Y. Enrichment of Geogenic Ammonium in Quaternary Alluvial–Lacustrine Aquifer Systems: Evidence from Carbon Isotopes and DOM Characteristics. *Environ. Sci. Technol.* **2020**, *54* (10), 6104–6114.

(5) Stoliker, D. L.; Repert, D. A.; Smith, R. L.; Song, B.; LeBlanc, D. R.; McCobb, T. D.; Conaway, C. H.; Hyun, S. P.; Koh, D.-C.; Moon, H. S.; Kent, D. B. Hydrologic Controls on Nitrogen Cycling Processes and Functional Gene Abundance in Sediments of a Groundwater Flow-Through Lake. *Environ. Sci. Technol.* **2016**, *50* (7), 3649–3657.

(6) Liang, Y.; Ma, R.; Nghiem, A.; Xu, J.; Tang, L.; Wei, W.; Prommer, H.; Gan, Y. Sources of Ammonium Enriched in Groundwater in the Central Yangtze River Basin: Anthropogenic or Geogenic? *Environ. Pollut.* **2022**, *306*, 119463.

(7) Sun, L.; Liang, X.; Jin, M.; Ma, B.; Zhang, X.; Song, C. Ammonium and Nitrate Sources and Transformation Mechanism in the Quaternary Sediments of Jianghan Plain, China. *Sci. Total Environ.* **2021**, *774*, 145131.

(8) Hansen, B.; Thorling, L.; Schullehner, J.; Termansen, M.; Dalgaard, T. Groundwater Nitrate Response to Sustainable Nitrogen Management. *Sci. Rep.* **2017**, *7* (1), 8566.

(9) Gao, Y.; Tian, Y.; Zhan, W.; Li, L.; Sun, H.; Zhao, T.; Zhang, H.; Meng, Y.; Li, Y.; Liu, T.; Ding, J. Characterizing Legacy Nitrogen-Induced Time Lags in Riverine Nitrogen Reduction for the Songhuajiang River Basin: Source Analysis, Spatio-Seasonal Patterns, and Impacts on Future Water Quality Improvement. *Water Res.* **2023**, *242*, 120292.

(10) Van Meter, K. J.; Basu, N. B.; Van Cappellen, P. Two Centuries of Nitrogen Dynamics: Legacy Sources and Sinks in the Mississippi and Susquehanna River Basins. *Global Biogeochem. Cycles* **2017**, *31* (1), 2–23.

(11) Van Meter, K. J.; Basu, N. B.; Veenstra, J. J.; Burras, C. L. The Nitrogen Legacy: Emerging Evidence of Nitrogen Accumulation in Anthropogenic Landscapes. *Environ. Res. Lett.* **2016**, *11* (3), 035014.

(12) Zhang, Y.-C.; Prommer, H.; Broers, H. P.; Slomp, C. P.; Greskowiak, J.; van der Grift, B.; Van Cappellen, P. Model-Based Integration and Analysis of Biogeochemical and Isotopic Dynamics in a Nitrate-Polluted Pyritic Aquifer. *Environ. Sci. Technol.* **2013**, *47* (18), 10415–10422.

(13) Liang, Y.; Ma, R.; Wang, Y.; Wang, S.; Qu, L.; Wei, W.; Gan, Y. Hydrogeological Controls on Ammonium Enrichment in Shallow Groundwater in the Central Yangtze River Basin. *Sci. Total Environ.* **2020**, *741*, 140350.

(14) Liu, Y.; Liu, C.; Nelson, W. C.; Shi, L.; Xu, F.; Liu, Y.; Yan, A.; Zhong, L.; Thompson, C.; Fredrickson, J. K.; Zachara, J. M. Effect of Water Chemistry and Hydrodynamics on Nitrogen Transformation Activity and Microbial Community Functional Potential in Hyporheic Zone Sediment Columns. *Environ. Sci. Technol.* **2017**, *51* (9), 4877–4886.

(15) Smith, R. L.; Repert, D. A.; Underwood, J. C.; Böhlke, J. K.; LeBlanc, D. R.; Hull, R. B.; Kent, D. B.; Reed, A. P.; Mroczkowski, S. J. Spatial, Seasonal, and Diel Controls of Nitrogen-Carbon-Oxygen Cycling During Lake-Water Infiltration to an Aquifer. *J. Geophys. Res. Biogeosci.* **2024**, *129* (4), No. e2023JG007659.

(16) Böhlke, J. K.; Smith, R. L.; Miller, D. N. Ammonium Transport and Reaction in Contaminated Groundwater: Application of Isotope Tracers and Isotope Fractionation Studies. *Water Resour. Res.* **2006**, *42*, 5.

(17) Covatti, G.; Grischek, T. Sources and Behavior of Ammonium during Riverbank Filtration. *Water Res.* **2021**, *191*, 116788.
(18) Santos, I. R.; Chen, X.; Lecher, A. L.; Sawyer, A. H.; Moosdorf, N.; Rodellas, V.; Tamborski, J.; Cho, H.-M.; Dimova, N.; Sugimoto, R.; Bonaglia, S.; Li, H.; Hajati, M.-C.; Li, L. Submarine Groundwater Discharge Impacts on Coastal Nutrient Biogeochemistry. *Nat. Rev. Earth Environ.* **2021**, *2* (5), 307−323.
(19) Johnson, H. M.; Stets, E. G. Nitrate in Streams During Winter Low-Flow Conditions as an Indicator of Legacy Nitrate. *Water Resour. Res.* **2020**, *56* (11), No. e2019WR026996.
(20) Wang, J.; Bai, J.; Zhao, Q.; Lu, Q.; Xia, Z. Five-Year Changes in Soil Organic Carbon and Total Nitrogen in Coastal Wetlands Affected by Flow-Sediment Regulation in a Chinese Delta. *Sci. Rep.* **2016**, *6* (1), 21137.
(21) Xie, H.; Wang, S.; Qiu, Z.; Jiang, J. Adsorption of NH4+-N on Chinese Loess: Non-Equilibrium and Equilibrium Investigations. *J. Environ. Manage.* **2017**, *202*, 46−54.
(22) Boatman, C. D.; Murray, J. W. Modeling Exchangeable NH4+ Adsorption in Marine Sediments: Process and Controls of Adsorption1,2. *Limnol. Oceanogr.* **1982**, *27* (1), 99−110.
(23) Triska, F. J.; Jackman, A. P.; Duff, J. H.; Avanzino, R. J. Ammonium Sorption to Channel and Riparian Sediments: A Transient Storage Pool for Dissolved Inorganic Nitrogen. *Biogeochemistry* **1994**, *26*, 67−83.
(24) Ceazan, M. L.; Thurman, E. M.; Smith, R. L. Retardation of Ammonium and Potassium Transport through a Contaminated Sand and Gravel Aquifer: The Role of Cation Exchange. *Environ. Sci. Technol.* **1989**, *23* (11), 1402−1408.
(25) Jiang, Q.; Jin, G.; Tang, H.; Xu, J.; Jiang, M. Ammonium (NH4+) Transport Processes in the Riverbank under Varying Hydrologic Conditions. *Sci. Total Environ.* **2022**, *826*, 154097.
(26) Rosenfeld, J. K. Ammonium Adsorption in Nearshore Anoxic Sediments1. *Limnol. Oceanogr.* **1979**, *24* (2), 356−364.
(27) Liu, R.; Ma, T.; Zhang, D.; Lin, C.; Chen, J. Spatial Distribution and Factors Influencing the Different Forms of Ammonium in Sediments and Pore Water of the Aquitard along the Tongshun River, China. *Environ. Pollut.* **2020**, *266*, 115212.
(28) Norrman, J.; Sparrenbom, C. J.; Berg, M.; Dang, D. N.; Jacks, G.; Harms-Ringdahl, P.; Pham, Q. N.; Rosqvist, H. Tracing Sources of Ammonium in Reducing Groundwater in a Well Field in Hanoi (Vietnam) by Means of Stable Nitrogen Isotope (Δ15N) Values. *Appl. Geochem.* **2015**, *61*, 248−258.
(29) Blackburn, T. H.; Henriksen, K. Nitrogen Cycling in Different Types of Sediments from Danish Waters1. *Limnol. Oceanogr.* **1983**, *28* (3), 477−493.
(30) Han, J.; Xu, J.; Yi, L.; Chang, Z.; Wang, J.; Ma, H.; Zhang, B.; Jiang, H. Seasonal Interaction of River Water-Groundwater-Salt Lake Brine and Its Influence on Water-Salt Balance in the Nalenggele River Catchment in Qaidam Basin, NW China. *J. Earth Sci.* **2022**, *33* (5), 1298−1308.
(31) Hu, Y.; Sun, Z.; Ma, R. Springs Emerging along the Elevation Gradient Indicate Intensive Groundwater-Surface Water Exchange in an Alpine Headwater Catchment, Northwestern China. *J. Earth Sci.* **2023**, *34* (1), 181−193.
(32) Ma, R.; Chen, K.; Andrews, C. B.; Loheide, S. P.; Sawyer, A. H.; Jiang, X.; Briggs, M. A.; Cook, P. G.; Gorelick, S. M.; Prommer, H.; Scanlon, B. R.; Guo, Z.; Zheng, C. Methods for Quantifying Interactions Between Groundwater and Surface Water. *Annu. Rev. Environ. Resour.* **2024**, *49*, 623.
(33) Ma, R.; Zheng, C.; Liu, C.; Greskowiak, J.; Prommer, H.; Zachara, J. M. Assessment of Controlling Processes for Field-Scale Uranium Reactive Transport under Highly Transient Flow Conditions. *Water Resour. Res.* **2014**, *50* (2), 1006−1024.
(34) Gu, C.; Anderson, W.; Maggi, F. Riparian Biogeochemical Hot Moments Induced by Stream Fluctuations. *Water Resour. Res.* **2012**, *48*, 9.
(35) Wang, J.; Ma, R.; Guo, Z.; Qu, L.; Yin, M.; Zheng, C. Experiment and Multicomponent Model Based Analysis on the Effect of Flow Rate and Nitrate Concentration on Denitrification in Low-Permeability Media. *J. Contam. Hydrol.* **2020**, *235*, 103727.
(36) Yabusaki, S. B.; Wilkins, M. J.; Fang, Y.; Williams, K. H.; Arora, B.; Bargar, J.; Beller, H. R.; Bouskill, N. J.; Brodie, E. L.; Christensen, J. N.; Conrad, M. E.; Danczak, R. E.; King, E.; Soltanian, M. R.; Spycher, N. F.; Steefel, C. I.; Tokunaga, T. K.; Versteeg, R.; Waichler, S. R.; Wainwright, H. M. Water Table Dynamics and Biogeochemical Cycling in a Shallow, Variably-Saturated Floodplain. *Environ. Sci. Technol.* **2017**, *51* (6), 3307−3317.
(37) Shuai, P.; Cardenas, M. B.; Knappett, P. S. K.; Bennett, P. C.; Neilson, B. T. Denitrification in the Banks of Fluctuating Rivers: The Effects of River Stage Amplitude, Sediment Hydraulic Conductivity and Dispersivity, and Ambient Groundwater Flow. *Water Resour. Res.* **2017**, *53* (9), 7951−7967.
(38) Castaldo, G.; Visser, A.; Fogg, G. E.; Harter, T. Effect of Groundwater Age and Recharge Source on Nitrate Concentrations in Domestic Wells in the San Joaquin Valley. *Environ. Sci. Technol.* **2021**, *55* (4), 2265−2275.
(39) Wallis, I.; Hutson, J.; Davis, G.; Kookana, R.; Rayner, J.; Prommer, H. Model-Based Identification of Vadose Zone Controls on PFAS Mobility under Semi-Arid Climate Conditions. *Water Res.* **2022**, *225*, 119096.
(40) Barnes, R. T.; Sawyer, A. H.; Tight, D. M.; Wallace, C. D.; Hastings, M. G. Hydrogeologic Controls of Surface Water-Groundwater Nitrogen Dynamics Within a Tidal Freshwater Zone. *J. Geophys. Res. Biogeosci.* **2019**, *124* (11), 3343−3355.
(41) Huang, K.; Liu, Y.; Yang, C.; Duan, Y.; Yang, X.; Liu, C. Identification of Hydrobiogeochemical Processes Controlling Seasonal Variations in Arsenic Concentrations Within a Riverbank Aquifer at Jianghan Plain, China. *Water Resour. Res.* **2018**, *54* (7), 4294−4308.
(42) Xue, P.; Wen, Z.; Zhao, D.; Jakada, H.; Liang, X. Determination of Hydraulic Conductivity and Its Spatial Variability in the Jianghan Plain Using a Multi-Format, Multi-Method Approach. *J. Hydrol.* **2021**, *594*, 125917.
(43) Schaefer, M. V.; Ying, S. C.; Benner, S. G.; Duan, Y.; Wang, Y.; Fendorf, S. Aquifer Arsenic Cycling Induced by Seasonal Hydrologic Changes within the Yangtze River Basin. *Environ. Sci. Technol.* **2016**, *50* (7), 3521−3529.
(44) Zhang, J.; Liang, X.; Jin, M.; Ma, T.; Deng, Y.; Ma, B. Identifying the Groundwater Flow Systems in a Condensed River-Network Interfluve between the Han River and Yangtze River (China) Using Hydrogeochemical Indicators. *Hydrogeol. J.* **2019**, *27* (7), 2415−2430.
(45) Vazquez, A.; López, M.; Kortaberria, G.; Martín, L.; Mondragon, I. Modification of Montmorillonite with Cationic Surfactants. Thermal and Chemical Analysis Including CEC Determination. *Appl. Clay Sci.* **2008**, *41* (1), 24−36.
(46) Zhou, Z.; Fu, Q.-L.; Fujii, M.; Waite, T. D. Complementary Elucidation of the Molecular Characteristics of Groundwater Dissolved Organic Matter Using Ultrahigh-Resolution Mass Spectrometry Coupled with Negative- and Positive-Ion Electrospray Ionization. *Environ. Sci. Technol.* **2023**, *57* (11), 4690−4700.
(47) Jiang, X.; Ma, R.; Ma, T.; Sun, Z. Modeling the Effects of Water Diversion Projects on Surface Water and Groundwater Interactions in the Central Yangtze River Basin. *Sci. Total Environ.* **2022**, *830*, 154606.
(48) Harbaugh, A. W. *MODFLOW-2005, The U.S. Geological Survey Modular Ground-Water Model-The Ground-Water Flow Process.* http://water.usgs.gov/software/ground_water.html/.
(49) Prommer, H.; Barry, D. A.; Zheng, C. MODFLOW/MT3DMS-Based Reactive Multicomponent Transport Modeling. *Groundwater* **2003**, *41* (2), 247−257.
(50) Prommer, H.; Tuxen, N.; Bjerg, P. L. Fringe-Controlled Natural Attenuation of Phenoxy Acids in a Landfill Plume: Integration of Field-Scale Processes by Reactive Transport Modeling. *Environ. Sci. Technol.* **2006**, *40* (15), 4732−4738.
(51) Haerens, B.; Prommer, H.; Lerner, D. N.; Dassargues, A. *Reactive Transport Modelling of a Groundwater Contamination by Ammoniacal Liquor*; University of Liège, 2006.

(52) Engelhardt, I.; Prommer, H.; Schulz, M.; Vanderborght, J.; Schüth, C.; Ternes, T. A. Reactive Transport of Iomeprol during Stream-Groundwater Interactions. *Environ. Sci. Technol.* **2014**, *48* (1), 199−207.
(53) Wallace, C. D.; Sawyer, A. H.; Barnes, R. T.; Soltanian, M. R.; Gabor, R. S.; Wilkins, M. J.; Moore, M. T. A Model Analysis of the Tidal Engine That Drives Nitrogen Cycling in Coastal Riparian Aquifers. *Water Resour. Res.* **2020**, *56* (4), No. e2019WR025662.
(54) Greskowiak, J.; Prommer, H.; Massmann, G.; Nützmann, G. Modeling Seasonal Redox Dynamics and the Corresponding Fate of the Pharmaceutical Residue Phenazone During Artificial Recharge of Groundwater. *Environ. Sci. Technol.* **2006**, *40* (21), 6615−6621.
(55) Greskowiak, J.; Prommer, H.; Vanderzalm, J.; Pavelic, P.; Dillon, P. Modeling of Carbon Cycling and Biogeochemical Changes during Injection and Recovery of Reclaimed Water at Bolivar, South Australia. *Water Resour. Res.* **2005**, *41*, 10.
(56) Schaefer, M. V.; Guo, X.; Gan, Y.; Benner, S. G.; Griffin, A. M.; Gorski, C. A.; Wang, Y.; Fendorf, S. Redox Controls on Arsenic Enrichment and Release from Aquifer Sediments in Central Yangtze River Basin. *Geochim. Cosmochim. Acta* **2017**, *204*, 104−119.
(57) Duan, Y.; Gan, Y.; Wang, Y.; Liu, C.; Yu, K.; Deng, Y.; Zhao, K.; Dong, C. Arsenic Speciation in Aquifer Sediment under Varying Groundwater Regime and Redox Conditions at Jianghan Plain of Central China. *Sci. Total Environ.* **2017**, *607−608*, 992−1000.
(58) Qiao, W.; Guo, H.; He, C.; Shi, Q.; Zhao, B. Unraveling Roles of Dissolved Organic Matter in High Arsenic Groundwater Based on Molecular and Optical Signatures. *J. Hazard. Mater.* **2021**, *406*, 124702.
(59) de Graaf, I. E. M.; Gleeson, T.; Rens van Beek, L. P. H.; Sutanudjaja, E. H.; Bierkens, M. F. P. Environmental Flow Limits to Global Groundwater Pumping. *Nature* **2019**, *574* (7776), 90−94.
(60) Brunner, P.; Cook, P. G.; Simmons, C. T. Hydrogeologic Controls on Disconnection between Surface Water and Groundwater. *Water Resour. Res.* **2009**, *45*, 1.
(61) Wang, W.; Chen, Y.; Wang, W.; Zhu, C.; Chen, Y.; Liu, X.; Zhang, T. Water Quality and Interaction between Groundwater and Surface Water Impacted by Agricultural Activities in an Oasis-Desert Region. *J. Hydrol.* **2023**, *617*, 128937.
(62) Ilampooranan, I.; Van Meter, K. J.; Basu, N. B. A Race Against Time: Modeling Time Lags in Watershed Response. *Water Resour. Res.* **2019**, *55* (5), 3941−3959.

https://doi.org/10.1021/acs.est.4c05015
Environ. Sci. Technol. XXXX, XXX, XXX−XXX